HHS Public Access

Author manuscript

Retina. Author manuscript; available in PMC 2019 March 01.

Published in final edited form as:

Retina. 2018 March ; 38(3): 445–461. doi:10.1097/IAE.0000000000001946.

Optical coherence tomography and histology of age-related macular degeneration support mitochondria as reflectivity sources

Katie M. Litts, PhD[1,2], **Yuhua Zhang, PhD**[1], **K. Bailey Freund, MD**[3], and **Christine A. Curcio, PhD**[1]

[1]Department of Ophthalmology, University of Alabama School of Medicine, Birmingham, Alabama, USA

[2]Department of Ophthalmology & Visual Sciences, Medical College of Wisconsin, Milwaukee, Wisconsin, USA

[3]Vitreous Retina Macula Consultants of New York, New York, USA

Abstract

Widespread adoption of optical coherence tomography (OCT) has revolutionized the diagnosis and management of retinal disease. If the cellular and subcellular sources of reflectivity in OCT can be identified, the value of this technology will be advanced even further towards precision medicine, mechanistic thinking, and molecular discovery. Four hyperreflective outer retinal bands are created by the exquisite arrangement of photoreceptors, Müller cells, retinal pigment epithelium, and Bruch's membrane. Due to massed effects of these axially compartmentalized and transversely aligned cells, reflectivity can be localized to the subcellular level. This review focuses on the second of the four bands, called ellipsoid zone (EZ) in a consensus clinical lexicon, with the central thesis that mitochondria in photoreceptor inner segments are a major independent reflectivity source in this band, due to Mie scattering and waveguiding. Our principal new data pertain to outer retinal tubulation, a unique neurodegenerative and gliotic structure with a highly reflective border, prominent in late age-related macular degeneration. High-resolution histology and multimodal imaging of this border together provide evidence that inner segment mitochondria undergoing fission and translocation towards the nucleus provide the reflectivity signal. We review the evolution of nomenclature, the ultrastructure and refractile properties of participating cells, what is revealed about photoreceptor inner segments by different detection technologies, and directions for future research. We conclude that our data support adoption of the EZ nomenclature. Identifying subcellular signal sources will newly inform clinical decision-making.

Keywords

Photoreceptors; Müller cells; age-related macular degeneration; outer retinal tubulation; ellipsoid; myoid; inner segments; reflectivity; optical coherence tomography; histology; transmission electron microscopy; adaptive optics

Corresponding Address: Christine A. Curcio, PhD; EyeSight Foundation of Alabama Vision Research Laboratories; Department of Ophthalmology; University of Alabama School of Medicine; 1670 University Boulevard Room 360; Birmingham AL 35294-0099; Ph 205.937.3785; F 205.934.3425; curcio@uab.edu.

Introduction

Optical coherence tomography (OCT), now ubiquitous in ophthalmology, is an interferometry technique that employs a low coherence light source to achieve noninvasive depth-resolved views of chorioretinal structure *in vivo*. In an OCT image, the depth information of the tissue structure is extracted from patterns formed by interference of light backscattered from the tissue and from a reference beam.[1] The structure and reflectivity of tissues and cells, in principle, are established by boundaries in refractive index.

Due to excellent depth resolution (7 μm in commercially available devices), reflectivity can be localized to the subcellular level in OCT images.[2] Four hyperreflective bands from the outer retina (Figure 1) are used to assess photoreceptors and their support system. Band terminology from an international working group is being widely adopted[3]: Band 1 (External Limiting Membrane; ELM), Band 2 (Ellipsoid Zone; EZ), Band 3 (Interdigitation Zone; IZ), and Band 4 (Retinal Pigment Epithelium (RPE)/Bruch's Membrane Complex). These bands (and the hyporeflective bands between them) are created by the spatial arrangement of Müller cells, photoreceptors, RPE, and Bruch's membrane. With subcellular resolution, the contributing cells are rendered with biologically distinct internal structures separated in depth, a feature best documented for the photoreceptors but also true for the RPE and Müller cells.[4–7]

The significance of OCT reflectivity can be elucidated with information afforded by high magnification and resolution histological investigation. Definitive imaging-histology correlations in the outer retina require attached and axially aligned photoreceptors, a challenge even in laboratory animals due to the potential for artefactual detachment and compaction of delicate outer segments. Further, commonly used animal models lack a macula (i.e., an all-cone foveola, sharp gradients of photoreceptor density, a Henle fiber layer,[8, 9] and a high concentration of Müller cells[10]). In contrast, in human eyes, pathology strongly perturbs outer retinal band structure on OCT, facilitating a qualitative match to histology. Prior to our recent publications,[11–17] the small number of human and monkey eyes examined in service of validating OCT included few pathologic specimens, non-macular tissues, few or imprecisely specified macular locations, and low-resolution OCT images.[18–24] OCT nomenclature maybe anatomically and neurologically informative.[25, 26]

In this article, we review the evolution of Band 2 nomenclature over the last two decades. We discuss the origins of imaging signals from photoreceptor mitochondria that could make molecular pathways in these organelles visible *in vivo*. In healthy eyes, mitochondria are uniquely arranged in a tight bundle in photoreceptor inner segments (IS) and comprise 74–85% of IS ellipsoid (ISel) volume in cones and 54–55% in rods.[27] Due to this abundance, mitochondria were proposed to perform optical functions in addition to canonical functions of oxidative phosphorylation and calcium buffering.[27] We review normal anatomy and optical properties of human outer retina. We present outer retinal tubulation (ORT) in age-related macular degeneration (AMD) as a probe of reflectivity. We discuss the debate on the ellipsoid zone versus inner segment/outer segment (IS/OS) nomenclature and technical considerations underlying conflicting data. We describe experimental and clinical studies

bearing on reflectivity and discuss strengths, limitations, and future directions. Taken together our recent data suggest that ISel mitochondria are a major reflectivity signal in OCT. For other aspects of OCT-revealed outer retinal structure, readers are directed to recent reviews.[28–30]

Evolution of Band 2 and its nomenclature

Early OCT, due to limited depth resolution, combined signals from adjacent retinal layers, resulting in one thick outer retinal reflective band.[31] As OCT technology improved in speed and resolution, new systems resolved outer retinal layers in more detail. By 1999, photoreceptors were visible as well as the RPE and choroid.[32] In 2004, a reflective band between Band 2 and the RPE became visible.[33] With newly revealed structures, terminology was adjusted accordingly.

To document evolving nomenclature for Band 2, we reviewed 164 published articles illustrating labeled OCT scans in normal macula in 7 major journals from 1995 to 2015. Several epochs are summarized in Table 1. Up to 2013 (through time-domain and spectral domain (SD) OCT), the most common name for Band 2 was IS/OS junction, which was based on internally inconsistent reflectivity data from one laboratory.[19, 34, 35] During this time, Huang et al directly aligned histology of photoreceptor layers and reflective bands in an avian eye, suggesting the ISel as one of several possible reflectivity sources.[32] Others also pointed out this correspondence.[36]

In 2011, to determine the dimensions of cellular compartments that regulate band spacing, Spaide and Curcio compiled outer retinal biometry from a century of published literature. The resulting anatomically precise model was aligned with the SDOCT bands from one instrument and anchored at Bands 1 and 4, which were felt to be secure. In the fovea and perifovea, Band 2 aligned best with the anatomical ISel and not the IS/OS.[11] Starting in 2012, ISel and EZ terminology appeared in publications, and references to the IS/OS decreased markedly.

In 2014, a comprehensive OCT nomenclature was proposed for all chorioretinal structures, and building on the Spaide and Curcio model, Band 2 was designated as EZ.[3] The term “zone” signified that factors beyond the anatomical ISel contributed to reflectivity and merited further research. Also in 2014, Jonnal et al,[37] using adaptive optics (AO)-assisted OCT imaging of individual cone photoreceptors, showed thin reflective planes at the Band 2 level. These were attributed to interfaces between cone IS and OS,[37] prompting commentary[38] and a debate that continues (see below).

In 2015, with OCT angiography on the rise,[39] numerous publications did not label the outer retinal bands, even if visible (Table 1), but in those that did, Band 2 was named EZ or ISel.

Origins of imaging signals: general principles and application to photoreceptors

Either in *en face* (e.g., scanning laser ophthalmoscopy, SLO) or cross-sectional (OCT) imaging, retinal structure is rendered by light scattered back to the detection device.[40] For high-resolution imaging to achieve maximal utility in elucidating disease progression, it is important to understand what subcellular structures contribute to reflectivity and how the

reflectivity is detected by different devices. Reflectivity is a collective manifestation of light scattering, i.e., the redirection of light from an original direction. Light as electromagnetic waves scatter when they meet an object. Simultaneously electric charges in the object are also excited by the electric field of the incident wave and re-radiate energy over a wide range of angles. Light propagation can be described by Maxwell's equations, which consider the interactions between the electric and magnetic fields of light with matter.[41, 42] Mie scattering is one solution of Maxwell's equations under specific conditions of particle size, shape, and refractive index, refractive index of the surrounding medium, and wavelength of light.[43, 44] Investigators have used Mie principles to model the effect of light passing through cells and tissues. In cultured cells, mitochondria and lysosomes are strong light scatterers, complying with Mie theory.[45–47] Below we will show that mitochondria are the main light scattering organelle in cone photoreceptor IS surviving in advanced AMD.

Light scattering by mitochondria is related to their functional status and morphology, making it possible to contemplate monitoring mitochondrial health *in vivo*. Scattering has been found to be proportional to the activity of succinate dehydrogenase (complex II of the electron transport chain and part of the Krebs cycle) and organelle content in normal and neoplastic tissues.[48] Refractivity of isolated mitochondria *in vitro* is affected by metabolic state.[49] Light scattering is affected by morphologic changes associated with oxidative stress.[45, 47] Further, mitochondrial morphology is dynamically controlled to respond to energy needs and environmental stimuli. Fission, resulting in smaller mitochondria, occurs in apoptotic cells and has been monitored in cultured cells by changes in light scattering,[50–52] with increased scattering/reflectivity/backscatter detectable by OCT.[53] Changes in mitochondrial ultrastructure, including an expanded matrix and absence of intra-cristal spaces, has been accompanied by a decrease in the ratio of wide-to-narrow angle scattering.[54]

Light scattering by photoreceptors also has a strong component over a narrow solid angle, known as waveguiding.[55–57] Light waveguiding can be mostly seen in an optical fiber which has a core of high refractive index relative to the surrounding medium, thereby allowing light to propagate by total internal reflection in patterns of energy distribution called modes.[55, 57] Photoreceptors are optical fibers, due to the internal packing geometry and high refractive index of ISel mitochondria.[58] In a normal eye, photoreceptors point to the pupil center.[59–61] Light returned from photoreceptors toward this center has a peaked intensity distribution called the optical Stiles–Crawford effect. In AO-assisted imaging, waveguiding allows high contrast imaging of the mosaic of photoreceptors.[56] Confocal AOSLO can efficiently collect light waveguided from the photoreceptors over a narrow angle, whereas AOSLO with non-confocal split-detection can collect light scattered from photoreceptors over wide angles. Thus, this modality can reveal photoreceptors even if waveguiding is absent due to cellular degeneration.[62]

Anatomy and optical properties of the outer retina in humans

Photoreceptors, Müller glia, and RPE are the cells of outer neurosensory retina (Figure 2). Cones and rods span from the outer plexiform layer to the apical side of the RPE. Light passes through the photoreceptors from the inner aspect (i.e., from synaptic terminal) to the

OS. Visual signal transmission flows in the opposite direction, from the OS to the synaptic terminal. Photoreceptor OS are made of stacked discs, and their tips are surrounded by specialized apical processes of the RPE.[63] OS are connected to IS by connecting cilia (Figure 3 insets). IS comprise inner and outer components of myoid (ISmy) and ISel. ISel house tightly packed bundles of mitochondria needed for high metabolism.[64] IS pass through the ELM and connect to photoreceptor nuclei in the outer nuclear layer (ONL). Cone and rod inner fibers interleaved with Müller cell fibers constitute the Henle fibers, unique to macula, and connect to cone pedicles and rod spherules, respectively. Photoreceptor OS and IS are surrounded by an extracellular matrix sheath containing cone- and rod-specific glycoconjugates.[65, 66] Müller cells, with somas in the inner nuclear layer and spanning all retinal layers,[67] contribute to junctional complexes with photoreceptors that comprise the ELM.[68]

The remainder of this review focuses on the bacillary layer,[69] i.e., the IS and OS of the rods and cones. However, recall that the hyporeflective ONL band in OCT comprises not only the anatomical ONL of photoreceptor nuclei but also the Henle fiber layer,[11, 70] which are distinguished from each other in normal eyes using directional OCT and in diseased eyes by hyperreflective patches in the inner 'ONL' often associated with focal pathology like drusen.[70] Readers may consult recent publications on this topic.[11, 70–72]

Human photoreceptors in excised tissues can be viewed by differential interference contrast microscopy to reveal differences in refractive index. In well-preserved tissues these observations provide a glimpse of *in vivo* optical properties.[73] Archival videos were available from a 1990 study of flat-mounted human retina that provided the histologic basis of single photoreceptor imaging via AOSLO.[62, 73, 74] Online Videos 1–3 reveal differences in cell shape, internal structure, and contrast along the IS long axis at two foveal and one perifoveal location. At the edge of the rod-free zone and the apex of cone ISel (near the OS, online Video 1), optical cross-sections are circular, widely separated by intervening interphotoreceptor matrix, and packed in an orderly triangular array. Further sclerad, IS cross-sections are large, polygonal, and contiguous with their neighbors, and they exhibit a finely granular internal structure consistent with packed mitochondria. At the ISmy, IS are wide, individual cells are barely resolvable, and internal texture is heterogeneous due to the presence of organelles including cone lipofuscin.[75, 76] At the ELM, IS cross-sections formed by tapered ISmy surrounded by Müller cell microvilli are again separated and circular. Importantly, the direction of contrast at the ELM is reversed from that in the ISel. That is, each cell is bright on its right side at the ISel and bright on its left side at the ELM. In the direction traveled by light (ELM, ISmy, ISel, OS), the refractive index gradients established at the ISmy, where cells are first individually resolvable, are maintained throughout the rest of the light path. Similar effects can be seen for the perifovea, where rods surround cones (online Video 2). Conversely, at the foveal center (online Video 3), cone IS are bright on the left edge at both the ISel and ELM. The absence of contrast reversal seen at other retinal locations is undetectable at the foveal center, suggesting different gradients of refractive index at this critical location for human vision.[27, 77]

These optical changes can be correlated with internal ultrastructure of IS as revealed by transmission electron microscopy of a macaque monkey macula (methods available in the

Supplementary information). Viewed in cross-section through the ISel near the myoid (Figure 3A,B) and near the OS (Figure 3C,D), mitochondria are electron-dense and tightly packed. In individual cones, ISel mitochondria are 7.3-fold more abundant near the myoid and 4.5-fold more abundant near the OS in the fovea compared to the perifovea.[9] Relative to the ISel near the myoid, the ISel near the OS had 39.9% fewer mitochondria in perifoveal regions. In rods, mitochondria number varied little across the macula (Figure 4A). Near the myoid and near the OS, the diameter of mitochondrial cross-sections and electron density are consistent in foveal and perifoveal regions. The cross-sectional area fraction occupied by mitochondria (an unbiased estimator of volume fraction) rises from 0.05 to 0.5 near myoid and 0.2 to 0.5 near OS (Figure 4B). To characterize the distribution of mitochondria across the IS cross-section,[78] mitochondria were counted in 5 annuli centered on the ISel geometric center (Figure 4C). Numerical density decreased from the ISel center to the perimeter in the apex (near OS) in fovea and perifovea, and was constant in the base (near myoid) until the last elliptical annular zone in foveal and perifoveal regions (zone 3 and zone 5, respectively). Conversely, the average diameter of a connecting cilium, the anatomical IS/OS, is just 0.37 μm (Figure 3D). A cross-section of connecting cilium encountered by incoming light is very small, making this structure an unlikely contributor of significant reflectivity.

Outer retinal tubulation as a probe of reflectivity

Our research program has access to high-quality human eye pathology specimens through a long-term collaboration with the Alabama Eye Bank, a large eye bank and a United States industry-leader in rapid tissue recovery. Because AMD is prevalent among older persons who may become eye donors, the potential for imaging-histology comparisons (between series of cases) and correlations (within single cases) for AMD is high. Between 1995–2009, we accessioned eyes for AMD research at <6 hr death-to- preservation time. In 2011–2013, NIH and foundation support enabled creation of the Project MACULA website, an online digital catalog of high-resolution histology of 82 AMD and 60 unremarkable aged maculae with an accessible database of annotations and layer thicknesses. The website was premised on the idea that subcellular detail was available in comprehensive structural SDOCT, and that histological validation of SDOCT could leverage longitudinal data in patient populations for accurate AMD timeline and pathobiology discovery. Among the insights afforded by systematic and unbiased review of these eyes was a major description of outer retinal tubulation (ORT), a form of neurodegeneration and gliosis first illustrated by author CAC in 1996[79] and named for its appearance in SDOCT by author KBF in 2009.[80] Histological insights were paired with multimodal imaging including optimized structural SDOCT and AOSLO.

It is useful to briefly review literature on neurodegeneration in AMD. Our long-standing hypothesis is that AMD is a disease of the photoreceptor support system (RPE and choroid) with a secondary neurodegeneration. Photoreceptor degeneration and death is the basis of visual dysfunction, and the relative rate and topography of rod and cone dysfunction is characteristic of every disease affecting photoreceptors. The human macula consists of a small foveal region (0.8 mm diameter) with only cones surrounded by a larger rod-dominated perifoveal annulus (6 mm outer diameter).[73, 81] Rods not only exist in the macula but also significantly predominate over cones (9:1 in a young adult, 6:1 in an older adult). In

aging and in early AMD, the parafovea and perifovea are susceptible to rod loss, with subsequent cone disease,[79, 82] as borne out by functional studies.[83, 84] Other histological studies of AMD eyes have demonstrated that as cones begin to degenerate, OS and IS shorten,[85] cone opsin redistributes,[86] and stress proteins are expressed. Cells dwindle in number over drusen[87] and undergo apoptosis.[88] Cones can persist without IS and OS over areas depleted of RPE in geographic atrophy.[89, 90]

Associated with advanced macular diseases affecting the RPE and especially late AMD, ORT is also found in some inherited retinopathies.[12, 80, 91–95] By SDOCT, ORT is a hyperreflective circular or ovoid profile surrounding a hyporeflective center in the ONL (Figure 5D) and distinguishable from cysts, which are mostly found in the inner retina and not surrounded by hyperreflectivity.[80] Clinically, ORT is seen as a biomarker for disease progression and can be stable over years.[96] ORT does not respond to anti-vascular endothelial growth factor therapy[96, 97] and portends a poor visual outcome due to outer retinal damage.[91] In eyes with ORT, areas of geographic atrophy were found to enlarge more slowly in one study[98] and more rapidly in another,[99] when compared to eyes lacking ORT.

The originators of ORT terminology speculated that ORT comprised scrolled photoreceptors,[80] and by histology, ORT is indeed a formation of degenerating photoreceptors and Müller cells forming the ELM (Figure 5B, also see Figure 6 from Litts el al[13]). Fluid-filled cysts lack this cellular organization.[17] Early studies of photoreceptor degeneration in AMD showed photoreceptors surviving in interconnecting tubes over disciform scars.[79] Evidence that photoreceptors forming ORT are largely cones is threefold. First, they are positive for carbonic anhydrase, a marker for cones expressing red or green opsin and for Müller cells.[79] Second, ORT has numerous spherical nuclei with euchromatin (cones) versus rare ovoid nuclei with heterochromatin (rods).[17] Third, in one case, every photoreceptor passing through the ELM contained one lipofuscin granule, distinct in size and staining from RPE lipofuscin[13] and characteristic of cone ISmy.[75] ORT is distinguished from the rosettes of retinoblastoma and other tumors by their tubular structure, large size, and degenerative instead of developmental nature.[17] ORT is also distinguished from rosettes in retinitis pigmentosa by RPE degeneration, location within the macula, and preponderance of surviving cones.[100, 101]

The ELM that forms ORT is linked to the border of outer retinal atrophy in AMD,[102] where the ELM descends towards Bruch's membrane, along with subsidence of the ONL.[14, 103, 104] The ELM descent has been classified in a recent histologic analysis of donor eyes with geographic atrophy and macular atrophy secondary to neovascularization.[105] Shapes of the ELM descent were termed flat, curved, and reflected, with the latter plausibly representing proximate steps in the formation of ORT. In a retrospective longitudinal study, atrophic borders progressing to ORT showed shorter elapsed time between the stages of reflected and scrolled ELM descent compared to atrophic borders not progressing to ORT.[12] Thus the presence of a scrolled ELM descent may represent a committed step of ORT formation. In eyes with neovascularization, those that progressed to ORT had shorter time between the steps of flat and curved than non-progressing borders. Variable progression rate between steps may underlie the apparent discrepancy in geographic atrophy growth rates between clinical studies.[98, 99]

As macular rods die preferentially in normal aging,[79] and only cones remain in ORT, the beginning and endpoints of this form of neurodegeneration are now established. Using openings in the ELM as a surrogate for cone IS diameter, we estimated spatial density (cells/mm^2) of cones surviving in ORT. Using the reflective ORT band, we calculated the total area inside ORT for a macula, and then the total number of ORT cones. In 10 eyes, we estimated that 6 to 44% of the cones present in a healthy macula were still present in ORT, depending on the eye.[13] The photoreceptor mosaic normally ranges from near 200,000 cells/mm^2 in the foveal center and ~10,000 cells/mm^2 at the macular perimeter in young adults.[73] Thus, the mean density of 20,351 cones/mm^2 in ORT suggests considerable distortion of this mosaic by Müller cell-driven remodeling.[13]

To explore the subcellular basis of ORT reflectivity, we defined 4 histological phases of cone degeneration: nascent (with OS), mature (without OS), degenerate (without IS), and end stage (no photoreceptors and Müller cells forming a circle of ELM).[17] A direct clinicopathologic correlation between clinical SDOCT and histology of ORT in one AMD case established mitochondria as the one organelle present in shrinking cone IS.[14] As cones degenerate inside and outside ORT, IS mitochondria change in both morphology and distribution (Figure 6).[14, 15] They undergo the process of fission (breaking apart), and they translocate towards the nucleus. Waveguiding towards the pupil center by ORT cones is unlikely, because the cones around ORT lumens are radially aligned. Mitochondria are thus implicated as independent reflectivity sources via scattering. However, they are not the only source for ORT, because translocating mitochondria cross the ELM and thus the reflective border of ORT incorporates both of these elements, dominated by the numerous mitochondria. The hyperreflective ORT band serves as a potent counterexample to the hypothesis that Band 2 represents the anatomical IS/OS junction. A refractive index boundary and/or change of the waveguiding properties between IS and OS does not seem likely in the absence of OS.

Is it EZ or IS/OS? Technical rationale underlying the debate

Although the EZ terminology is being widely used (Table 1), many authors continue with IS/OS nomenclature. Here, we summarize evidence suggesting that there may be a common ground, if we consider the principles of different imaging modalities including SDOCT and AO-assisted imaging. AO imaging employs a wavefront sensor to measure wave aberrations of the imaging light caused by the eye, and a deformable mirror to correct aberrations, thereby improving retinal image quality.[106–109]

SDOCT and AO-OCT findings: Meadway et al, using AO-OCT, obtained a thickness of 6 μm for Band 2 for a sample of 100 cones at 2°–3° eccentricity and interpreted them as correlating to the ISel.[110] In this study the foveal reflex, a single surface reflector, was found to be 4.8 μm, less than the calculated Band 2 thickness. Thus, Band 2 was thicker than could be explained by a single surface reflection but was not as thick as the entire anatomical ISel.[110] In a second study, SDOCT and a novel Reflectivity Model Based (RefMoB) method to fit Gaussian functions of linear reflectivities was used to measure thickness and vertical positions of the outer retinal bands in normal maculae.[111] Band 2 measured 11.6 μm at the foveal center, 6.0–6.1 μm at ±1500 μm eccentricity in the foveal scan, and 5.9–6.5 μm across

the perifoveal scan. These data were compared to histology of 18 normal human maculae, and Band 2 reflections were attributed to the outer one-third of the ISel.[111] Thus, these two studies together suggested that Band 2 reflectivity arose from the anatomical ISel but probably not its entire length, perhaps just the outer portion with the tapered tip. In a third study, using AO-OCT, Jonnal et al measured the thickness of 9593 individual cones' contributions to Band 2 at 2° (~600 μm) and 5° (~1500 μm) eccentricity and found that the thickness (4.7 μm) was close to a single reflective plane.[37] SDOCT blurred these reflections, resulting in a reflective band that was three times thicker.[37] These authors proposed that a slanted interface between the plasma membranes of the IS and OS could provide a single reflective plane in AO-OCT, thus justifying the IS/OS name.[37] Jonnal et al concluded that the ~15 μm-ellipsoid does not generate band 2, because the band was too narrow by a factor of 4 and too distant from the ELM.

The debate: The Jonnal model[37] gave rise to a correspondence by Spaide[38] and a reply.[112] Four points were raised in this interchange. First, it is possible that variation in the vertical position of photoreceptors could appear as a thick band in commercial SDOCT systems. Second, the cones analyzed by AO-OCT were highly subject to selection bias. Third, two studies using histology and older OCT technology had actually shown hypo- rather than hyperreflectivity at this interface. Fourth, rod photoreceptors were omitted from the AO-OCT reflectivity model. A debate like this is best solved with new data, which has not been forthcoming for normal eyes to date. A suggestion that IS/OS and EZ terms be used interchangeably[17] is unsatisfactory in our view, because the anatomical IS/OS junction (cilia, to a retinal cell biologist) and the ISel differ markedly in ultrastructure, protein content, and controlling genes[6, 113] as evidenced in inherited retinopathies affecting specific photoreceptor components.

We capitalized on new knowledge of ORT ultrastructure and visualized ORT in patients with atrophy using the distinct signal detection technologies of SDOCT and AOSLO.[16] Our rationale is shown schematically in Figure 7, and results from one case are shown in Figure 8. By confocal AOSLO, photoreceptors presumed to be waveguiding appear as bright spots in an array representing the mosaic of cones. These are thought to require OS integrity and contact with RPE apical processes corresponding to the IZ on OCT.[62, 114, 115] AOSLO imaging focuses light approximately on the ELM (red triangle, Figure 7A) and collects the reflected light by a double-pass through a large pupil. The light emerging from the cones originates from two primary reflections that occur within the optical fiber component of the cells, the first from the ISel, and the second at the interdigitation of OS and RPE apical processes.[114] Because of this large pupil, the cone numerical aperture is narrower than AOSLO numerical aperture (red triangle smaller than angle between lines, Figure 7B). All reflected light from a single cone is collected, and AOSLO renders a clear mosaic. Normally oriented photoreceptors give the maximal light signal thereby presenting well-aligned and uniform-appearing structures such as ELM and EZ by OCT. Degenerating cones with remnant or absent OS do not waveguide and thus the visibility of photoreceptor mosaic by AOSLO (Figure 7C) and EZ band by OCT is diminished.

To image the retinas of patients with ORT, we used an AOSLO device specifically designed for older persons who may have small pupils, compromised media, and poor fixation.[116]

Figure 8 shows multimodal panoramic and detailed imaging of a patient with geographic atrophy secondary to AMD. A branched ORT was visible on near-infrared reflectance imaging (Figure 8B, F) and by *en face* OCT, (Figure 8C, G) this ORT appeared bright. In contrast, this same ORT was dark in AOSLO, even though cones in unaffected areas of the macula were hyperreflective. (Figure 8E) We interpret these findings to mean that SDOCT detects scattering by persistent mitochondria with coherently enhanced imaging signal, whereas the waveguiding that enables high contrast cone visualization in AOSLO has been abolished. Further, because ORT cone IS contain many dispersed mitochondria, which reflect light (red arrows, Figure 7D), OCT renders ORT with a hyperreflective border, whereas by AOSLO, ORT cones appear dark. By AO-OCT, Panorgias et al showed images of ORT in an eye with geographic atrophy.[117] These authors attributed reflectivity in photoreceptor bands exclusively to waveguiding but did not offer a mechanism for the visibility of ORT.

ORT has provided a new perspective on photoreceptor optics. It is important to remember that two major hypotheses for the correlate of Band 2 rely on different light contributing mechanisms (scattering over wide and narrow angles) and image formation (coherent enhancement in OCT). Different technologies may be tapping into different parts of the same larger truth about photoreceptor optics.

Experimental and clinical studies of EZ reflectivity

Band thickness and reflectivity measurements are subject to errors that should be considered when evaluating the expanding EZ literature. First, reflectivity generated by OCT instruments are contrast-adjusted (in logarithm scale) so that low-intensity features are visible to a human observer. Simulations[111, 118] show that this adjustment not only systematically thickens Bands 1–4 but also moves the vertical positions of Bands 3–4, in opposite directions. Thus, measurements made from contrast-adjusted data must be viewed cautiously. Conversely, automated segmentation using linear reflectivity may or may not delineate bands correctly if pathology is present. Also, reflectivity of individual bands should be checked for image variability by comparison to features in the same scan that are less affected by the disease process.[119] Because Müller cells span the retina, finding uninvolved structures between the internal and external limiting membranes for normalization may be challenging.

OCT is now available for animal models (Figure 9), and species with outer retinas of interest for validating signal sources include ground squirrels whose ISel mitochondria scramble during hibernation,[120] tree shrews with mega-mitochondria,[121] and mice with genetic mutations impacting OS fine structure.[122] In frog retina, investigated with a high-resolution line scan OCT and subsequent histology using a fluorescent marker for mitochondria,[123] the ratio of distances Band 2-Band 1 to Band 1-OPL (by OCT) and IS/OS-ELM to ELM-OPL (by histology) differed significantly, indicating Band 2 did not correspond to the anatomical IS/OS. In monkeys, after a light flash, Band 2 intensity decreased, while the intensity between Band 2 and 3 increased, suggesting structural and functional differences for both ISel and OS.[124]

The EZ attracts interest because of a potential correlation with visual acuity and prognostic value in retinal diseases.[17] In macular telangiectasia type 2, reduced rhodopsin immunoreactivity in rods corresponded with Band 2 loss seen by clinical OCT, while specific marker proteins in mitochondria, cones, and the ELM were unchanged, prompting the idea that rod loss degrades cone reflectivity by causing misalignment.[125] In a comprehensive review incorporating insights from laboratory studies of photoreceptor degeneration, Mitamura et al suggested that the timeline of retinitis pigmentosa starts with Band 3 shortening and disappearance, and proceeds to Band 2 and Band 1 in order.[29] Longer extents of these bands correlated with better retinal sensitivity and visual acuity. Reduced band 2 intensity has been associated with decreased cone function in patients with early AMD,[126] achromatopsia,[127] and cone dystrophy.[128] Reduced intensity is also associated with hypopigmentation and large drusen in intermediate AMD, possibly indicating disease progression.[129]

Strengths, limitations, and future directions

1. Strengths of our ORT research include the confluence of a large number of post-mortem eyes with short death to preservation time viewed with high-resolution histology and *in vivo* multimodal imaging based on eye-tracked SDOCT and informed by AOSLO. Limitations include the fact that OCT does not yet provide enough details to determine cone degeneration phases described in ORT[17] or to disambiguate the contribution of reflectivity sources from ELM and mitochondria in the scrolling phase of ORT. Future studies of ORT should include directional OCT and split-detection AOSLO.

2. Despite these limitations, our data substantially validate mitochondria as the major reflectivity source for Band 2, supporting the consensus EZ nomenclature.[3]

3. Further, we proposed that the myoid zone of the consensus lexicon,[3] i.e., the hyporeflective band between the ELM and the inner aspect of the EZ, should be evaluated as a marker for cone degeneration, because as mitochondria translocate inward, the myoid decreases in length.[15]

4. New information on ORT learned from AMD is relevant to inherited retinopathies like choroideremia, which are in clinical trials for gene therapy. Clear optics of these overall younger patients can allow observation of detailed natural history of ORT formation and involution as well as the contribution of individual genes to the regulation of reflectivity.[95, 130] Importantly, understanding ORT precursors will be helpful in selecting patients most likely to benefit from treatment.

5. While ORT research has been extremely informative, we should extrapolate from pathology to normal retina cautiously. Our data do not exclude other factors such as the tapered IS apex, the cone matrix sheath, and the presence of rods as contributors to or modulators of reflectivity. Further, the EZ should be seen in the context of visualizing all photoreceptor parts, including OS relations to RPE

apical processes (IZ) and axons in relation to Müller cells in the Henle fiber layer. More research on all these points is welcome.

6. If mitochondria are plausible reflectors in the IS, then they are candidate reflectors elsewhere in the retina. Mitochondria are prominent in inner retinal neuronal cell bodies, synapses (especially the large pedicles of cone photoreceptors), and in Müller cell cytoplasm near vasculature.[5]

7. Mitochondrial fission, an important process of cell death in age-related neurodegenerations like Parkinson and Alzheimer disease, can be observed, with all that entails, *in vivo*. Fission is a process that sequesters irreparably damaged mitochondrial components for elimination by mitophagy, a bulk disposal process involving transport towards the soma.[131]

8. Animal models can be approached experimentally to determine the regulation of reflectivity. SDOCT devices have been available for the pre-clinical market since 2011, and a comprehensive naming of all the outer retinal bands is now available for mouse.[132] These will enable cell-to-cell correlations, like those done with human eyes[133] in animal models amenable to deep molecular analysis. Standardization will speed translation of laboratory results to clinical knowledge, and scientific questions of clinical importance to the laboratory.

9. Improved visualization of and metrics for mitochondrial health are possible, based on SDOCT coupled with metabolic imaging, e.g., via two-photon fluorescence.[134]

10. Comparing the results from SDOCT and AOSLO visualization of ORT emphasizes that to maximize clinical utility of these sophisticated techniques, we should understand the principles of the imaging technology.

11. Because photoreceptors are superior optical devices and geometrically precise, they are amenable to many analyses that will inform clinical diagnosis as well as reveal their remarkable biology.

Supplementary Material

Refer to Web version on PubMed Central for supplementary material.

Acknowledgments

We thank Jeffrey D. Messinger, DC for assistance with histology, and Larry Parmley for assistance with video production.

Financial Disclosures: This article substantively reviews PhD dissertation research that was supported by the Vision Science Graduate Program at UAB (KML). Dr. Zhang is supported by EY021903, EY024378, International Retina Research Foundation, and the EyeSight Foundation of Alabama. The Eye Donor Project and Dr. Freund's participation are supported by the Macula Foundation. Dr. Curcio is supported by International Retinal Research Foundation, unrestricted funds to the Department of Ophthalmology from Research to Prevent Blindness, Inc., and EyeSight Foundation of Alabama.

Acquisition of donor eyes for AMD research was supported by National Eye Institute (EY06109, P30 EY003039), International Retinal Research Foundation, and the Arnold and Mabel Beckman Initiative for Macular Research. The Project MACULA website was supported by these and additionally by the Edward N. and Della L. Thome Memorial Foundation. KBF is a Consultant to Genentech, Optos, Optovue, Heidelberg Engineering, and Spark

Therapeutics; Research support from Genentech/Roche. CAC is a Consultant to Novartis; Research support from Genentech/Roche, Heidelberg Engineering.

References

1. Adhi M, Duker JS. Optical coherence tomography - current and future applications. Curr Opin Ophthalmol. 2013; 24:213–221. [PubMed: 23429598]
2. Heidelberg Engineering. Spectralis Operating Instructions. Heidelberg, Germany: 2007. Ver. 001
3. Staurenghi G, Sadda S, Chakravarthy U, et al. Proposed lexicon for anatomic landmarks in normal posterior segment spectral-domain optical coherence tomography: the IN*OCT consensus. Ophthalmology. 2014; 121:1572–1578. [PubMed: 24755005]
4. Uga S, Smelser. Comparative study of the fine structure of retinal Muller cells in various vertebrates. Invest Ophthalmol. 1973; 12:434–448. [PubMed: 4541022]
5. Stone J, van Driel D, Valter K, et al. The locations of mitochondria in mammalian photoreceptors: relation to retinal vasculature. Brain Res. 2008; 1189:58–69. [PubMed: 18048005]
6. Borwein B, Borwein D, Medeiros J, McGowan JW. The ultrastructure of monkey foveal photoreceptors, with special reference to the structure, shape, size, and spacing of the foveal cones. Am J Anat. 1980; 159:125–146. [PubMed: 7446444]
7. Krebs W, Krebs I. Primate retina and choroid: Atlas of fine structure in man and monkey. New York: Springer Verlag; 1991.
8. Drasdo N, Millican CL, Katholi CR, Curcio CA. The length of Henle fibers in the human retina and a model of ganglion receptive field density in the visual field. Vision Res. 2007; 47:2901–2911. [PubMed: 17320143]
9. Polyak SL. The Vertebrate Visual System. Chicago: University of Chicago; 1957.
10. Burris C, Klug K, Ngo IT, et al. How Muller glial cells in macaque fovea coat and isolate the synaptic terminals of cone photoreceptors. J Comp Neurol. 2002; 453:100–111. [PubMed: 12357435]
11. Curcio CA, Messinger JD, Sloan KR, et al. Human chorioretinal layer thicknesses measured in macula-wide, high-resolution histologic sections. Invest Ophthalmol Vis Sci. 2011; 52:3943–3954. [PubMed: 21421869]
12. Dolz-Marco R, Litts KM, Tan ACS, et al. The evolution of outer retinal tubulation, a neurodegeneration and gliosis prominent in macular diseases. Ophthalmology. 2017
13. Litts KM, Ach T, Hammack KM, et al. Quantitative analysis of outer retinal tubulation in age-related macular degeneration from spectral-domain optical coherence tomography and histology. Invest Ophthalmol Vis Sci. 2016; 57:2647–2656. [PubMed: 27177321]
14. Litts KM, Messinger JD, Dellatorre K, et al. Clinicopathological correlation of outer retinal tubulation in age-related macular degeneration. JAMA Ophthalmol. 2015; 133:609–612. [PubMed: 25742505]
15. Litts KM, Messinger JD, Freund KB, et al. Inner segment remodeling and mitochondrial translocation in cone photoreceptors in age-related macular degeneration with outer retinal tubulation. Invest Ophthalmol Vis Sci. 2015; 56:2243–2253. [PubMed: 25758815]
16. Litts KM, Wang X, Clark ME, et al. Exploring photoreceptor reflectivity through multimodal imaging of outer retinal tubulation in advanced age-related macular degeneration. Retina. 2017; 37:978–988. [PubMed: 27584549]
17. Schaal KB, Freund KB, Litts KM, et al. Outer retinal tubulation in advanced age-related macular degeneration: optical coherence tomographic findings correspond to histology. Retina. 2015; 35:1339–1350. [PubMed: 25635579]
18. Toth CA, Narayan DG, Boppart SA, et al. A comparison of retinal morphology viewed by optical coherence tomography and by light microscopy. Arch Ophthalmol. 1997; 115:1425–1428. [PubMed: 9366674]
19. Anger EM, Unterhuber A, Hermann B, et al. Ultrahigh resolution optical coherence tomography of the monkey fovea. Identification of retinal sublayers by correlation with semithin histology sections. Exp Eye Res. 2004; 78:1117–1125. [PubMed: 15109918]

20. Chauhan DS, Marshall J. The interpretation of optical coherence tomography images of the retina. Invest Ophthalmol Vis Sci. 1999; 40:2332–2342. [PubMed: 10476800]
21. Chen TC, Cense B, Miller JW, et al. Histologic correlation of in vivo optical coherence tomography images of the human retina. Am J Ophthalmol. 2006; 141:1165–1168. [PubMed: 16765704]
22. Ghazi NG, Dibernardo C, Ying HS, et al. Optical coherence tomography of enucleated human eye specimens with histological correlation: origin of the outer “red line”. Am J Ophthalmol. 2006; 141:719–726. [PubMed: 16564808]
23. Brown NH, Koreishi AF, McCall M, et al. Developing SDOCT to assess donor human eyes prior to tissue sectioning for research. Graefes Arch Clin Exp Ophthalmol. 2009; 247:1069–1080. [PubMed: 19225801]
24. Bagheri N, Bell BA, Bonilha VL, Hollyfield JG. Imaging human postmortem eyes with SLO and OCT. Adv Exp Med Biol. 2012; 723:479–488. [PubMed: 22183367]
25. Cruz-Herranz A, Balk LJ, Oberwahrenbrock T, et al. The APOSTEL recommendations for reporting quantitative optical coherence tomography studies. Neurology. 2016; 86:2303–2309. [PubMed: 27225223]
26. Cameron JR, Albrecht P, Cruz-Herranz A, et al. The APOSTEL recommendations for reporting quantitative optical coherence tomography studies. Neurology. 2016; 87:1960.
27. Hoang QV, Linsenmeier RA, Chung CK, Curcio CA. Photoreceptor inner segments in monkey and human retina: mitochondrial density, optics, and regional variation. Vis Neurosci. 2002; 19:395–407. [PubMed: 12511073]
28. Wong IY, Iu LP, Koizumi H, Lai WW. The inner segment/outer segment junction: what have we learnt so far? Curr Opin Ophthalmol. 2012; 23:210–218. [PubMed: 22450219]
29. Mitamura Y, Mitamura-Aizawa S, Katome T, et al. Photoreceptor impairment and restoration on optical coherence tomographic image. J Ophthalmol. 2013; 2013:518170. [PubMed: 23691278]
30. Keane PA, Patel PJ, Liakopoulos S, et al. Evaluation of age-related macular degeneration with optical coherence tomography. Surv Ophthalmol. 2012; 57:389–414. [PubMed: 22898648]
31. Huang D, Swanson EA, Lin CP, et al. Optical coherence tomography. Science. 1991; 254:1178–1181. [PubMed: 1957169]
32. Huang Y, Cideciyan AV, Papastergiou GI, et al. Relation of optical coherence tomography to microanatomy in normal and rd chickens. Invest Ophthalmol Vis Sci. 1998; 39:2405–2416. [PubMed: 9804149]
33. Cense B, Nassif N, Chen T, et al. Ultrahigh-resolution high-speed retinal imaging using spectral-domain optical coherence tomography. Opt Express. 2004; 12:2435–2447. [PubMed: 19475080]
34. Drexler W, Sattmann H, Hermann B, et al. Enhanced visualization of macular pathology with the use of ultrahigh-resolution optical coherence tomography. Arch Ophthalmol. 2003; 121:695–706. [PubMed: 12742848]
35. Spaide RF. Questioning optical coherence tomography. Ophthalmology. 2012; 119:2203–2204 e2201. [PubMed: 23122463]
36. Fernández EJ, Hermann B, Povazay B, et al. Ultrahigh resolution optical coherence tomography and pancorrection for cellular imaging of the living human retina. Opt Express. 2008; 16:11083–11094. [PubMed: 18648422]
37. Jonnal RS, Kocaoglu OP, Zawadzki RJ, et al. The cellular origins of the outer retinal bands in optical coherence tomography images. Invest Ophthalmol Vis Sci. 2014; 55:7904–7918. [PubMed: 25324288]
38. Spaide RF. Outer retinal bands. Invest Ophthalmol Vis Sci. 2015; 56:2505–2506. [PubMed: 26066596]
39. Kashani AH, Lee SY, Moshfeghi A, et al. Optical coherence tomography angiography of retinal venous occlusion. Retina. 2015; 35:2323–2331. [PubMed: 26457395]
40. Optical Coherence Tomography: Technology and Applications. New York: Springer; 2008.
41. van de Hulst HC. Light scattering by small particles. New York: Dover Publications Inc; 1981.
42. Bohren CF, Huffman DR. Absorption and scattering of light by small particles. New York: John Wiley & Sons, Inc; 1998.

43. Quinten M. Optical properties of nanoparticle systems: Mie and beyond. New York: Wiley; 2011.
44. Wang LV, Wu H. Biomedical optics: Principles and imaging. New Jersey: John Wiley & Sons, Inc; 2007.
45. Wilson JD, Cottrell WJ, Foster TH. Index-of-refraction-dependent subcellular light scattering observed with organelle-specific dyes. J Biomed Opt. 2007; 12:014010. [PubMed: 17343485]
46. Wilson JD, Foster TH. Mie theory interpretations of light scattering from intact cells. Opt Lett. 2005; 30:2442–2444. [PubMed: 16196346]
47. Wilson JD, Bigelow CE, Calkins DJ, Foster TH. Light scattering from intact cells reports oxidative-stress-induced mitochondrial swelling. Biophys J. 2005; 88:2929–2938. [PubMed: 15653724]
48. Beauvoit B, Evans SM, Jenkins TW, et al. Correlation between the light scattering and the mitochondrial content of normal tissues and transplantable rodent tumors. Anal Biochem. 1995; 226:167–174. [PubMed: 7785769]
49. Tychinsky V. The metabolic component of cellular refractivity and its importance for optical cytometry. J Biophotonics. 2009; 2:494–504. [PubMed: 19644930]
50. Mulvey CS, Sherwood CA, Bigio IJ. Wavelength-dependent backscattering measurements for quantitative real-time monitoring of apoptosis in living cells. J Biomed Opt. 2009; 14:064013. [PubMed: 20059251]
51. Pasternack RM, Zheng JY, Boustany NN. Detection of mitochondrial fission with orientation-dependent optical Fourier filters. Cytometry A. 2011; 79:137–148. [PubMed: 21265007]
52. Pasternack RM, Zheng JY, Boustany NN. Optical scatter changes at the onset of apoptosis are spatially associated with mitochondria. J Biomed Opt. 2010; 15:040504. [PubMed: 20799771]
53. Farhat G, Mariampillai A, Yang VX, et al. Detecting apoptosis using dynamic light scattering with optical coherence tomography. J Biomed Opt. 2011; 16:070505. [PubMed: 21806246]
54. Zheng JY, Tsai YC, Kadimcherla P, et al. The C-terminal transmembrane domain of Bcl-xL mediates changes in mitochondrial morphology. Biophys J. 2008; 94:286–297. [PubMed: 17766334]
55. Enoch JM. Optical Properties of the Retinal Receptors. J Opt Soc Am. 1963; 53:71.
56. Roorda A, Williams DR. Optical fiber properties of individual human cones. J Vis. 2002; 2:404–412. [PubMed: 12678654]
57. Liu Z, Kocaoglu OP, Turner TL, Miller DT. Modal content of living human cone photoreceptors. Biomed Opt Express. 2015; 6:3378–3404. [PubMed: 26417509]
58. Rowe MP, Engheta N, Easter SS Jr, Pugh EN Jr. Graded-index model of a fish double cone exhibits differential polarization sensitivity. J Opt Soc Am A Opt Image Sci Vis. 1994; 11:55–70. [PubMed: 8106915]
59. Laties AM, Enoch JM. An analysis of retinal receptor orientation. I. Angular relationship of neighboring photoreceptors. Invest Ophthalmol. 1971; 10:69–77. [PubMed: 4992333]
60. Burns SA, Wu S, Delori F, Elsner AE. Direct measurement of human-cone-photoreceptor alignment. J Opt Soc Am A Opt Image Sci Vis. 1995; 12:2329–2338. [PubMed: 7500214]
61. Burns SA, Wu S, He JC, Elsner AE. Variations in photoreceptor directionally across the central retina. J Opt Soc Am A Opt Image Sci Vis. 1997; 14:2033–2040. [PubMed: 9291599]
62. Scoles D, Sulai YN, Langlo CS, et al. In vivo imaging of human cone photoreceptor inner segments. Invest Ophthalmol Vis Sci. 2014; 55:4244–4251. [PubMed: 24906859]
63. Steinberg RH, Wood I, Hogan MJ. Pigment epithelial ensheathment and phagocytosis of extrafoveal cones in human retina. Philos Trans R Soc Lond B Biol Sci. 1977; 277:459–474. [PubMed: 16301]
64. Rueda EM, Johnson JE Jr, Giddabasappa A, et al. The cellular and compartmental profile of mouse retinal glycolysis, tricarboxylic acid cycle, oxidative phosphorylation, and ~P transferring kinases. Mol Vis. 2016; 22:847–885. [PubMed: 27499608]
65. Fariss RN, Anderson DH, Fisher SK. Comparison of photoreceptor-specific matrix domains in the cat and monkey. Exp Eye Res. 1990; 51:473–485. [PubMed: 2209757]
66. Johnson LV, Hageman GS. Structural and compositional analyses of isolated cone matrix sheaths. Invest Ophthalmol Vis Sci. 1991; 32:1951–1957. [PubMed: 2055688]

67. Distler C, Dreher Z. Glia cells of the monkey retina – II. Müller cells. Vision Res. 1996; 36:2381–2394. [PubMed: 8917802]
68. Williams DS, Arikawa K, Paallysaho T. Cytoskeletal components of the adherens junctions between the photoreceptors and the supportive Muller cells. J Comp Neurol. 1990; 295:155–164. [PubMed: 2341633]
69. Polyak S. The Retina. Chicago: University of Chicago; 1941.
70. Lujan BJ, Roorda A, Knighton RW, Carroll J. Revealing Henle's fiber layer using spectral domain optical coherence tomography. Invest Ophthalmol Vis Sci. 2011; 52:1486–1492. [PubMed: 21071737]
71. Ouyang Y, Walsh AC, Keane PA, et al. Different phenotypes of the appearance of the outer plexiform layer on optical coherence tomography. Graefes Arch Clin Exp Ophthalmol. 2013; 251:2311–2317. [PubMed: 23661097]
72. Lujan BJ, Roorda A, Croskrey JA, et al. Directional optical coherence tomography provides accurate outer nuclear layer and henle fiber layer measurements. Retina. 2015; 35:1511–1520. [PubMed: 25829348]
73. Curcio CA, Sloan KR, Kalina RE, Hendrickson AE. Human photoreceptor topography. J Comp Neurol. 1990; 292:497–523. [PubMed: 2324310]
74. Zhang T, Godara P, Blanco ER, et al. variability in human cone topography assessed by adaptive optics scanning laser ophthalmoscopy. Am J Ophthalmol. 2015; 160:290–300 e291. [PubMed: 25935100]
75. Iwasaki M, Inomata H. Lipofuscin granules in human photoreceptor cells. Invest Ophthalmol Vis Sci. 1988; 29:671–679. [PubMed: 3366562]
76. Tucker GS. Refractile bodies in the inner segments of cones in the aging human retina. Invest Ophthalmol Vis Sci. 1986; 27:708–715. [PubMed: 3009350]
77. Yamada E. Some structural features of the fovea centralis of the human retina. Arch Ophthalmol. 1969; 82:151–159. [PubMed: 4183671]
78. Cameron DA, Pugh EN Jr. Double cones as a basis for a new type of polarization vision in vertebrates. Nature. 1991; 353:161–164. [PubMed: 1891046]
79. Curcio CA, Medeiros NE, Millican CL. Photoreceptor loss in age-related macular degeneration. Invest Ophthalmol Vis Sci. 1996; 37:1236–1249. [PubMed: 8641827]
80. Zweifel SA, Engelbert M, Laud K, et al. Outer retinal tubulation: A novel optical coherence tomography finding. Arch Ophthalmol. 2009; 127:1596–1602. [PubMed: 20008714]
81. Østerberg GA. Topography of the layer of rods and cones in the human retina. Acta Ophthalmol. 1935; 13(Suppl 6):1–103.
82. Curcio CA, Millican CL, Allen KA, Kalina RE. Aging of the human photoreceptor mosaic: Evidence for selective vulnerability of rods in central retina. Invest Ophthalmol Vis Sci. 1993; 34:3278–3296. [PubMed: 8225863]
83. Owsley C, McGwin G Jr, Clark ME, et al. Delayed rod-mediated dark adaptation is a functional biomarker for incident early age-related macular degeneration. Ophthalmology. 2016; 123:344–351. [PubMed: 26522707]
84. Owsley C, Jackson GR, White M, et al. Delays in rod-mediated dark adaptation in early age-related maculopathy. Ophthalmology. 2001; 108:1196–1202. [PubMed: 11425675]
85. Johnson PT, Lewis GP, Talaga KC, et al. Drusen-associated degeneration in the retina. Invest Ophthalmol Vis Sci. 2003; 44:4481–4488. [PubMed: 14507896]
86. Shelley EJ, Madigan MC, Natoli R, et al. Cone degeneration in aging and age-related macular degeneration. Arch Ophthalmol. 2009; 127:483–492. [PubMed: 19365029]
87. Johnson PT, Brown MN, Pulliam BC, et al. Synaptic pathology, altered gene expression, and degeneration in photoreceptors impacted by drusen. Invest Ophthalmol Vis Sci. 2005; 46:4788–4795. [PubMed: 16303980]
88. Dunaief JL, Dentchev T, Ying GS, Milam AH. The role of apoptosis in age-related macular degeneration. Arch Ophthalmol. 2002; 120:1435–1442. [PubMed: 12427055]
89. Bird AC, Phillips RL, Hageman GS. Geographic atrophy: a histopathological assessment. JAMA Ophthalmol. 2014; 132:338–345. [PubMed: 24626824]

90. Kim SY, Sadda S, Humayun MS, et al. Morphometric analysis of the macula in eyes with geographic atrophy due to age-related macular degeneration. Retina. 2002; 22:464–470. [PubMed: 12172114]

91. Lee JY, Folgar FA, Maguire MG, et al. Outer retinal tubulation in the comparison of age-related macular degeneration treatments trials (CATT). Ophthalmology. 2014; 121:2423–2431. [PubMed: 25064723]

92. Goldberg NR, Greenberg JP, Laud K, et al. Outer retinal tubulation in degenerative retinal disorders. Retina. 2013; 33:1871–1876. [PubMed: 23676993]

93. Iriyama A, Aihara Y, Yanagi Y. Outer retinal tubulation in inherited retinal degenerative disease. Retina. 2013; 33:1462–1465. [PubMed: 23538577]

94. Fujinami K, Sergouniotis PI, Davidson AE, et al. Clinical and molecular analysis of Stargardt disease with preserved foveal structure and function. Am J Ophthalmol. 2013; 156:487–501 e481. [PubMed: 23953153]

95. Sun LW, Johnson RD, Williams V, et al. multimodal imaging of photoreceptor structure in choroideremia. PLoS One. 2016; 11:e0167526. [PubMed: 27936069]

96. Jung JJ, Freund KB. Long-term follow-up of outer retinal tubulation documented by eye-tracked and en face spectral-domain optical coherence tomography. Arch Ophthalmol. 2012; 130:1618–1619. [PubMed: 23229712]

97. Wolff B, Maftouhi MQ, Mateo-Montoya A, et al. Outer retinal cysts in age-related macular degeneration. Acta Ophthalmol. 2011; 89:e496–499. [PubMed: 21631905]

98. Hariri A, Nittala MG, Sadda SR. Outer retinal tubulation as a predictor of the enlargement amount of geographic atrophy in age-related macular degeneration. Ophthalmology. 2015; 122:407–413. [PubMed: 25315664]

99. Moussa K, Lee JY, Stinnett SS, Jaffe GJ. Spectral domain optical coherence tomography-determined morphologic predictors of age-related macular degeneration-associated geographic atrophy progression. Retina. 2013; 33:1590–1599. [PubMed: 23538573]

100. Curcio CA, Allen KA, Sloan KR, et al. Distribution and morphology of human cone photoreceptors stained with anti-blue opsin. J Comp Neurol. 1991; 312:610–624. [PubMed: 1722224]

101. Tulvatana W, Adamian M, Berson EL, Dryja TP. Photoreceptor rosettes in autosomal dominant retinitis pigmentosa with reduced penetrance. Arch Ophthalmol. 1999; 117:399–402. [PubMed: 10088824]

102. Sarks SH. Ageing and degeneration in the macular region: a clinico-pathological study. Br J Ophthalmol. 1976; 60:324–341. [PubMed: 952802]

103. Zanzottera EC, Ach T, Huisingh C, et al. Visualizing retinal pigment epithelium phenotypes in the transition to geographic atrophy in age-related macular degeneration. Retina. 2016

104. Sayegh RG, Simader C, Scheschy U, et al. A systematic comparison of spectral-domain optical coherence tomography and fundus autofluorescence in patients with geographic atrophy. Ophthalmology. 2011; 118:1844–1851. [PubMed: 21496928]

105. Zanzottera EC, Ach T, Huisingh C, et al. Visualizing retinal pigment epithelium phenotypes in the transition to atrophy in neovascular age-related macular degeneration. Retina. 2016

106. Williams DR. Imaging single cells in the living retina. Vision Res. 2011; 51:1379–1396. [PubMed: 21596053]

107. Liang J, Williams DR, Miller DT. Supernormal vision and high-resolution retinal imaging through adaptive optics. J Opt Soc Am A Opt Image Sci Vis. 1997; 14:2884–2892. [PubMed: 9379246]

108. Miller DT, Williams DR, Morris GM, Liang J. Images of cone photoreceptors in the living human eye. Vision Res. 1996; 36:1067–1079. [PubMed: 8762712]

109. Roorda A, Duncan JL. Adaptive optics ophthalmoscopy. Annual Review of Vision Science. 2015; 1:19–50.

110. Meadway A, Girkin CA, Zhang Y. A dual-modal retinal imaging system with adaptive optics. Opt Express. 2013; 21:29792–29807. [PubMed: 24514529]

111. Ross DH, Clark ME, Godara P, et al. Refmob, a reflectivity feature model-based automated method for measuring four outer retinal hyperreflective bands in optical coherence tomography. Invest Ophthalmol Vis Sci. 2015; 56:4166–4176. [PubMed: 26132776]
112. Jonnal RS, Kocaoglu OP, Zawadzki RJ, et al. Author response: Outer retinal bands. Invest Ophthalmol Vis Sci. 2015; 56:2507–2510. [PubMed: 26066597]
113. Reidel B, Thompson JW, Farsiu S, et al. Proteomic profiling of a layered tissue reveals unique glycolytic specializations of photoreceptor cells. Mol Cell Proteomics. 2011; 10:M110 002469.
114. Putnam NM, Hammer DX, Zhang Y, et al. Modeling the foveal cone mosaic imaged with adaptive optics scanning laser ophthalmoscopy. Opt Express. 2010; 18:24902–24916. [PubMed: 21164835]
115. Jacob J, Paques M, Krivosic V, et al. Meaning of visualizing retinal cone mosaic on adaptive optics images. Am J Ophthalmol. 2015; 159:118–123 e111. [PubMed: 25284764]
116. Zhang Y, Wang X, Rivero EB, et al. Photoreceptor perturbation around subretinal drusenoid deposits as revealed by adaptive optics scanning laser ophthalmoscopy. Am J Ophthalmol. 2014; 158:584–596 e581. [PubMed: 24907433]
117. Panorgias A, Zawadzki RJ, Capps AG, et al. Multimodal assessment of microscopic morphology and retinal function in patients with geographic atrophy. Invest Ophthalmol Vis Sci. 2013; 54:4372–4384. [PubMed: 23696601]
118. Spaide RF, Curcio CA. Anatomical correlates to the bands seen in the outer retina by optical coherence tomography: literature review and model. Retina. 2011; 31:1609–1619. [PubMed: 21844839]
119. Charafeddin W, Nittala MG, Oregon A, Sadda SR. Relationship between subretinal hyperreflective material reflectivity and volume in patients with neovascular age-related macular degeneration following anti-vascular endothelial growth factor treatment. Ophthalmic Surg Lasers Imaging Retina. 2015; 46:523–530. [PubMed: 26057755]
120. Reme CE, Young RW. The effects of hibernation on cone visual cells in the ground squirrel. Invest Ophthalmol Vis Sci. 1977; 16:815–840. [PubMed: 893032]
121. Knabe W, Skatchkov S, Kuhn HJ. “Lens mitochondria” in the retinal cones of the tree-shrew Tupaia belangeri. Vision Res. 1997; 37:267–271. [PubMed: 9135860]
122. Bonilha VL, Bell BA, Rayborn ME, et al. Loss of DJ-1 elicits retinal abnormalities, visual dysfunction, and increased oxidative stress in mice. Exp Eye Res. 2015; 139:22–36. [PubMed: 26215528]
123. Lu R-W, Curcio CA, Zhang Y, et al. Investigation of the hyper-reflective ‘inner/outer segment’ band in optical coherence tomography of living frog retina. J Biomed Optics. 2012; 17:060504.
124. Suzuki W, Tsunoda K, Hanazono G, Tanifuji M. Stimulus-induced changes of reflectivity detected by optical coherence tomography in macaque retina. Invest Ophthalmol Vis Sci. 2013; 54:6345–6354. [PubMed: 23982841]
125. Powner MB, Gillies MC, Zhu M, et al. Loss of Muller’s cells and photoreceptors in macular telangiectasia type 2. Ophthalmology. 2013; 120:2344–2352. [PubMed: 23769334]
126. Wu Z, Ayton LN, Guymer RH, Luu CD. Second reflective band intensity in age-related macular degeneration. Ophthalmology. 2013; 120:1307–1308 e1301. [PubMed: 23732057]
127. Genead MA, Fishman GA, Rha J, et al. Photoreceptor structure and function in patients with congenital achromatopsia. Invest Ophthalmol Vis Sci. 2011; 52:7298–7308. [PubMed: 21778272]
128. Hood DC, Zhang X, Ramachandran R, et al. The inner segment/outer segment border seen on optical coherence tomography is less intense in patients with diminished cone function. Invest Ophthalmol Vis Sci. 2011; 52:9703–9709. [PubMed: 22110066]
129. Gin TJ, Wu Z, Chew SK, et al. Quantitative analysis of the ellipsoid zone intensity in phenotypic variations of intermediate age-related macular degeneration. Invest Ophthalmol Vis Sci. 2017; 58:2079–2086. [PubMed: 28388704]
130. Xue K, Oldani M, Jolly JK, et al. Correlation of optical coherence tomography and autofluorescence in the outer retina and choroid of patients with choroideremia. Invest Ophthalmol Vis Sci. 2016; 57:3674–3684. [PubMed: 27403996]

131. MacAskill AF, Kittler JT. Control of mitochondrial transport and localization in neurons. Trends Cell Biol. 2010; 20:102–112. [PubMed: 20006503]

132. DeRamus ML, Stacks DA, Zhang Y, et al. GARP2 accelerates retinal degeneration in rod cGMP-gated cation channel β-subunit knockout mice. Sci Rep. 2017; 7:42545. [PubMed: 28198469]

133. Balaratnasingam C, Messinger JD, Sloan KR, et al. Histologic and optical coherence tomographic correlates in drusenoid pigment epithelium detachment in age-related macular degeneration. Ophthalmology. 2017

134. Sharma R, Williams DR, Palczewska G, et al. Two-photon autofluorescence imaging reveals cellular structures throughout the retina of the living primate eyetwo-photon autofluorescence imaging. Invest Ophthalmol Vis Sci. 2016; 57:632–646. [PubMed: 26903224]

135. Monés J, Biarnes M, Trindade F. Hyporeflective wedge-shaped band in geographic atrophy secondary to age-related macular degeneration: an underreported finding. Ophthalmology. 2012; 119:1412–1419. [PubMed: 22440276]

136. Zanzottera EC, Messinger JD, Ach T, et al. The Project MACULA retinal pigment epithelium grading system for histology and optical coherence tomography in age-related macular degeneration. Invest Ophthalmol Vis Sci. 2015; 56:3253–3268. [PubMed: 25813989]

137. Flannery JG, Farber DB, Bird AC, Bok D. Degenerative changes in a retina affected with autosomal dominant retinitis pigmentosa. Invest Ophthalmol Vis Sci. 1989; 30:191–211. [PubMed: 2914751]

138. Wolff B, Matet A, Vasseur V, et al. En face oct imaging for the diagnosis of outer retinal tubulations in age-related macular degeneration. J Ophthalmol. 2012; 2012:542417. [PubMed: 22970349]

Summary Statement

We review evolution of terminology for the second of four hyperreflective outer retinal bands on optical coherence tomography and describe how the ellipsoid zone nomenclature is supported by recent data showing mitochondria to be a major independent reflectivity source in photoreceptor inner segments.

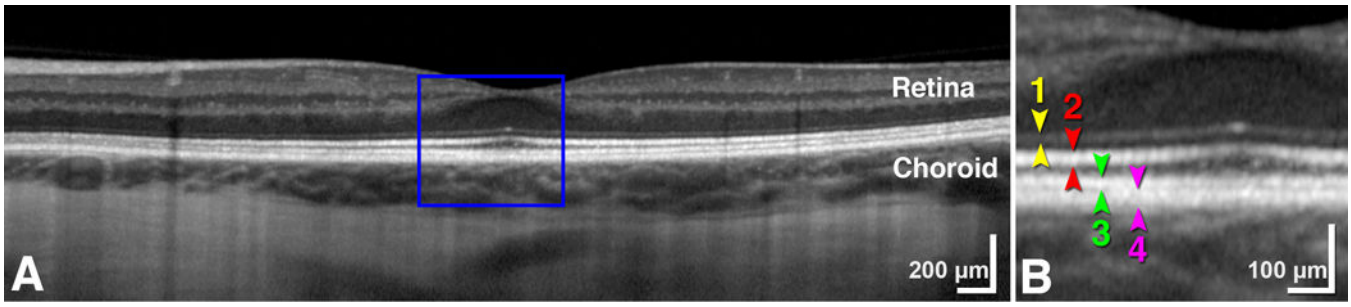

Figure 1. Hyperreflective outer retinal bands in spectral domain optical coherence tomography

A. SDOCT B-scan of a normal human retina and choroid. B. Higher magnification of blue box in A with hyperreflective bands indicated using consensus nomenclature[3]: 1, external limiting membrane; 2, ellipsoid zone; 3, interdigitation zone; 4, retinal pigment epithelium/ Bruch's complex.

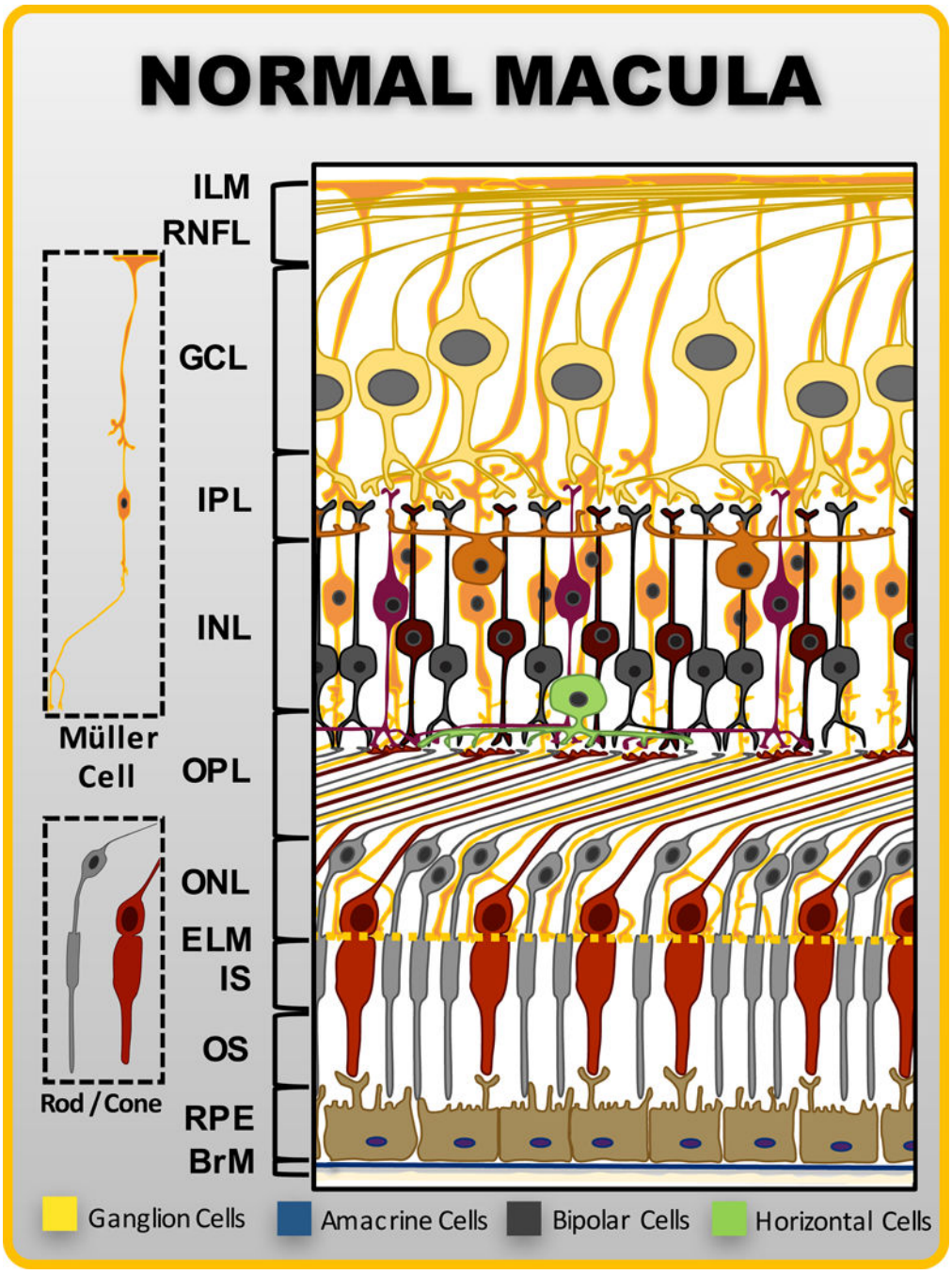

Figure 2. Cells contributing to outer retinal hyperreflective bands in normal macula

Schematic of normal retina highlighting the relationship between rod (gray) and cone (red) photoreceptors with Müller cells (orange, spanning from ELM to ILM). Foveal center is located off the left edge of the schematic. The Henle fiber layer courses centrifugally, from outer to inner. ILM, inner limiting membrane; RNFL, retinal nerve fiber layer; GCL, ganglion cell layer; IPL, inner plexiform layer; INL, inner nuclear layer; OPL, outer plexiform layer; ONL, outer nuclear layer; ELM, external limiting membrane; IS, inner

segments; OS, outer segments; RPE, retinal pigment epithelium; BrM, Bruch's membrane. Adapted from Dolz-Marco et al with permission.[12]

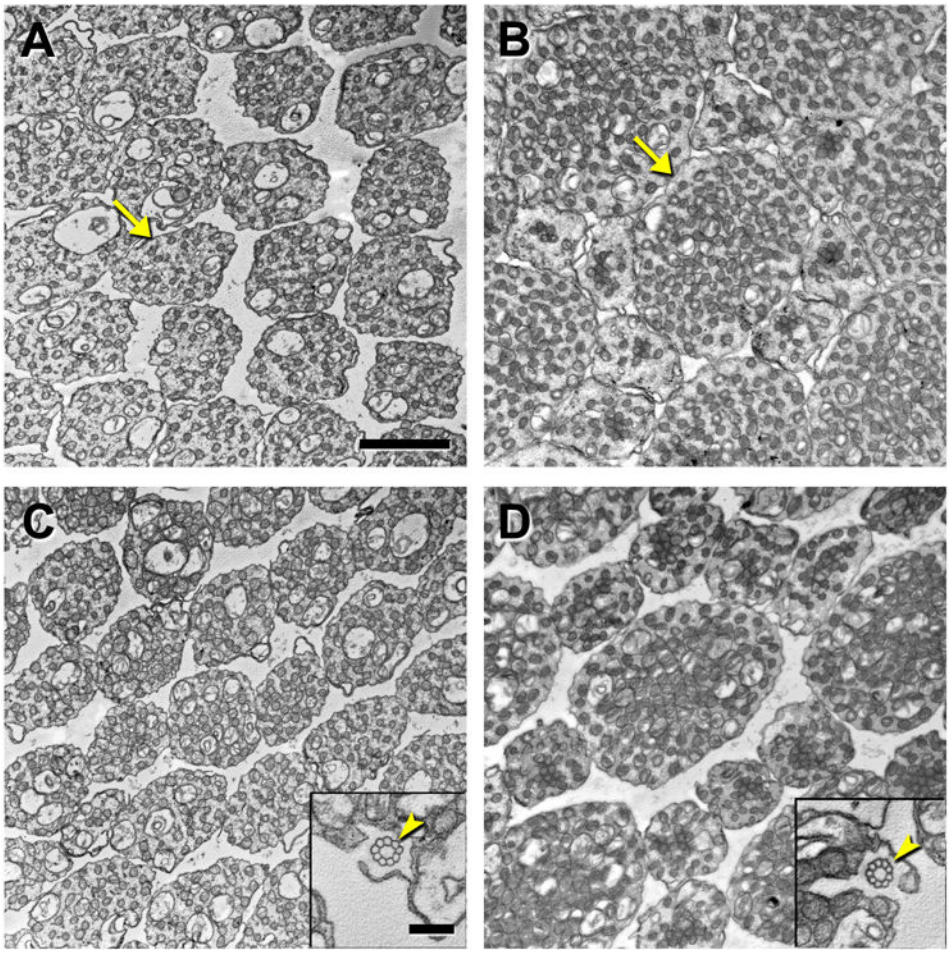

Figure 3. Inner segment ellipsoids in cross-section from macaque retina

Macaca Mulatta, 10-year-old male, transmission electron microscopy. Mitochondria (arrows) and cilia (arrowheads, insets). A, C. Fovea, ellipsoid base, near the myoid (A) and apex, near the OS (C). B, D. Perifovea, base (B) and apex (D) Scale bars, 0.5 μm.

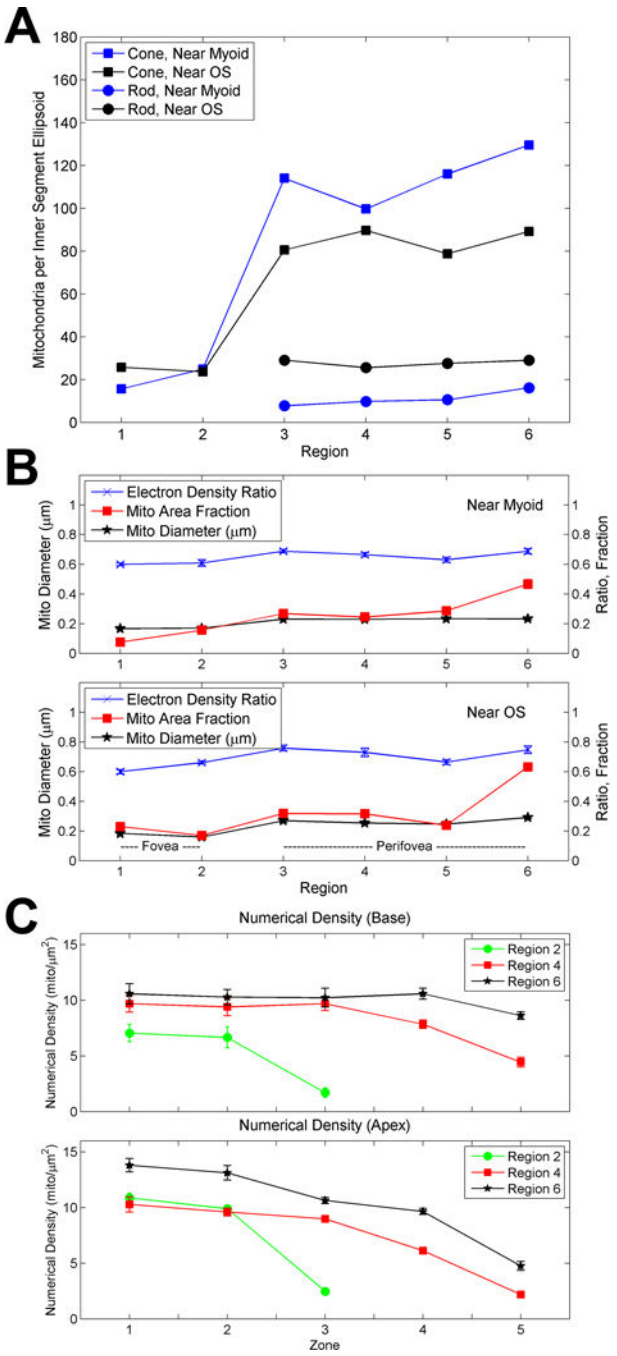

Figure 4. Mitochondrial abundance in inner segment ellipsoids

Retina of 10-year-old male Macaca Mulatta. A. Mitochondria per inner segment ellipsoid (ISel) in cones of rod-free regions (1–2 on x-axis) and cones and rods of perifoveal regions (3–6 on x-axis) in macaque. Standard error bars are smaller than the symbols. B. Diameter of mitochondria, mitochondria area fraction, and electron density for cone ISel in macaque. Bars, standard error. C. Numerical density of mitochondria in ISel as a function of distance from the ISel center, near myoid (top) and near OS (bottom), in macaque. Numerical density was calculated with 5 elliptical annular zones, centered on ISel geometric center with a

major radius of 0.475 μm and a minor radius of 0.375 μm. Each point in a region is an average of cones in 6 micrographs for that level. Zones 4 and 5 in Region 2 (fovea) have no mitochondria because they extend outside the diameter of the ellipsoid (2.04 μm for near OS). Regions 4 and 6, rod-containing perifovea. Bars, standard error.

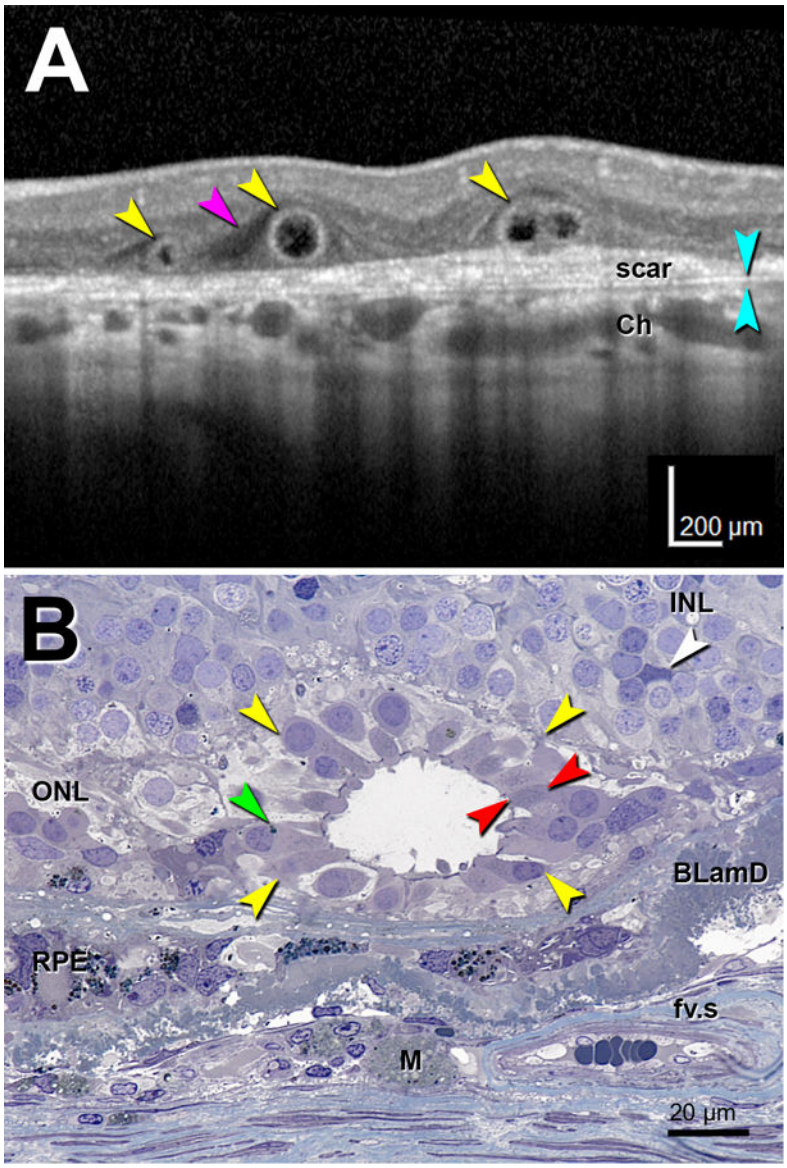

Figure 5. Histology and SDOCT imaging of outer retinal tubulation in age-related macular degeneration

Spectral domain optical coherence tomography (SDOCT) imaging and histology of outer retinal tubulation (ORT), in cross-sections (yellow arrowheads). (A) Representative SDOCT B-scan of three ORT cross-sections from an 81-year-old woman with neovascular AMD. Two closed ORTs on the left, and a branching ORT on the right. Hyporeflective wedge[135] (pink arrowhead); Bruch's membrane (cyan arrowheads). (B) High-resolution histology section of degenerate cones in ORT, at 1.5 mm from the fovea from a different 81- year-old woman with neovascular AMD. Cone lipofuscin (green arrowhead); mitochondria in outer fiber (red arrowheads); Muller cell body (white arrowhead). BLamD, basal laminar deposit; Ch, choroid; fv.s, fibrovascular scar; INL, inner nuclear layer; M, lipid- containing macrophage; RPE, 'entombed' and 'melanotic' retinal pigment epithelium (terminology of Zanzottera et al[136]). Used with permission from Litts et al.[13]

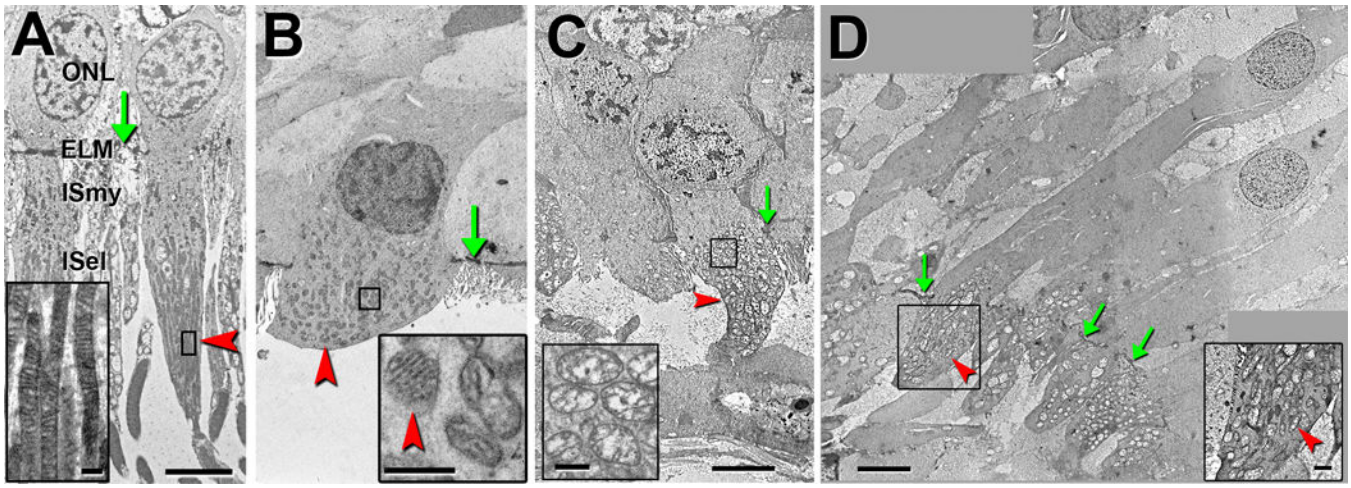

Figure 6. Ultrastructure of cone photoreceptors in age-related macular degeneration

Neovascular AMD, except where noted. Green arrows indicate ELM, and red arrowheads indicate mitochondria in all panels. A. Photoreceptors at 2.5 mm temporal to the foveal center in a healthy macula. Mitochondria are thin and tightly packed in the ISel (inset, magnified box). 85-year-old woman. B. Degenerating cone at 3 mm from the foveal center. Mitochondria are spherical, ovoid, or reniform (inset, magnified box).[137] 87-year-old woman. C. Outer retinal tubulation cone with long IS containing spherical mitochondria that have not translocated internally to the ELM (inset, magnified box). At 2.1 mm temporal from the foveal center. 77-year-old woman. D. Cone from mature ORT with nucleus retracted from ELM. Mitochondria in IS are ovoid (inset, magnified box). At 2 mm nasal from the foveal center. 87-year-old woman. Mitochondria in C and D are vacuolated due to post-mortem delay to fixation. ELM, external limiting membrane; ISel, photoreceptor inner segment ellipsoid; ISmy, photoreceptor inner segment myoid; ONL, outer nuclear layer. Scale bars: 5 μm (A-D); 250 nm (A,B insets); 1 μm (C,D insets). Adapted from Litts et al.[15]

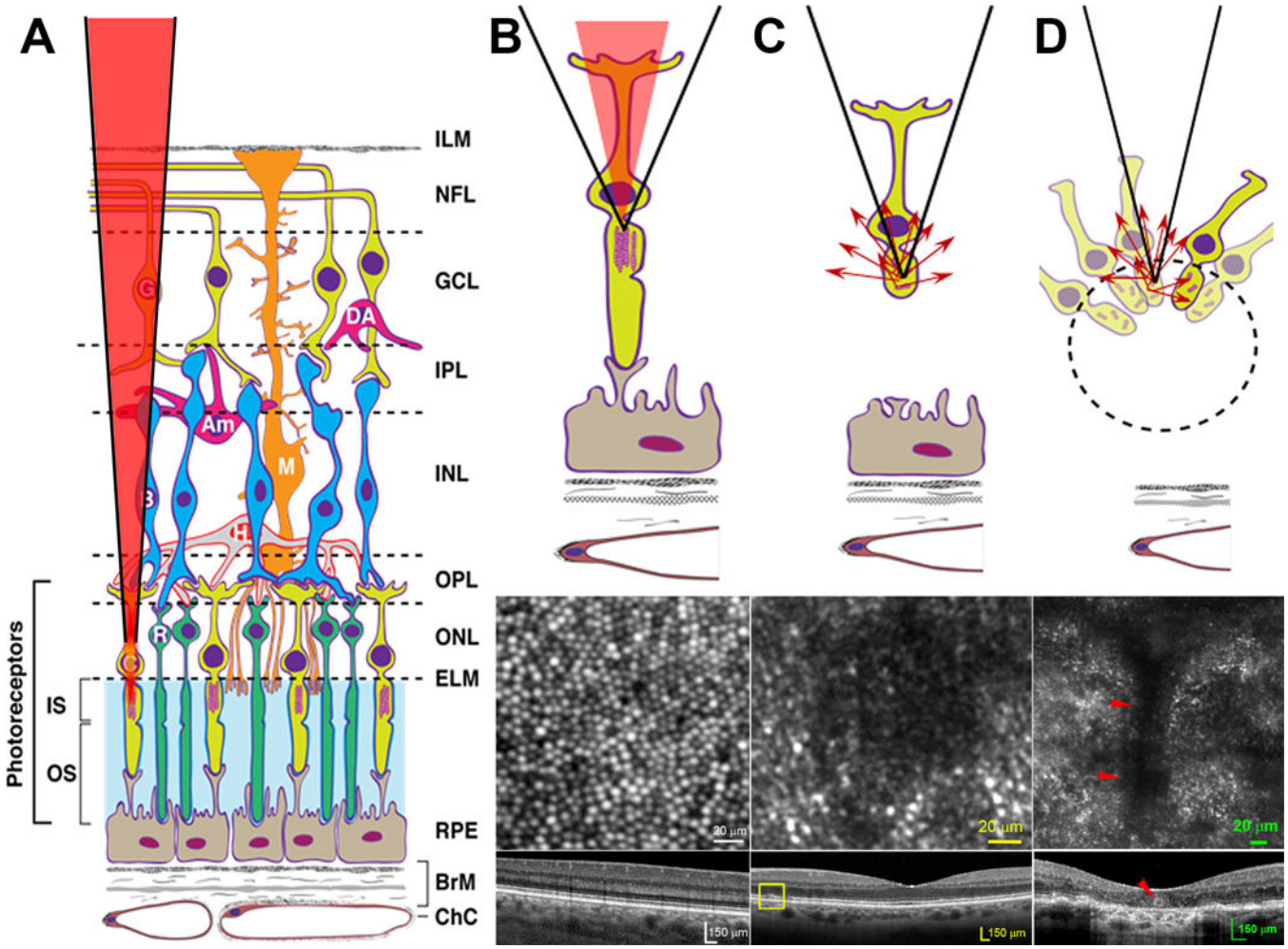

Figure 7. Multimodal imaging of normal and degenerating cones

A. In a normal eye, photoreceptors are oriented toward the pupil center, and inner segments (IS) contain bundles of long mitochondria. AOSLO illuminates cones by focusing light (as indicated by the red triangle) on the ELM and collects the reflected light, by a double pass through a large pupil. Due to waveguiding, light coupled inside the cone (within the cone's numerical aperture) traverses the outer segment and is scattered near the tip of the outer segment. Part of the scattered light is coupled back inside the outer segment and is guided back toward the pupil when it emerges from the photoreceptor IS. This part of the light is collected by either AOSLO or OCT. B. Because of this large pupil, the cone numerical aperture is narrower (red triangle) than AOSLO numerical aperture (angle between black lines). Reflected light is collected, and AOSLO renders a clear IS mosaic. C. Degenerating cones with remnant or absent OS do not waveguide but still have reflective organelles. These form a diffuse reflector, scattering incident light over a wide angle (red arrows). Only light within the AOSLO numerical aperture (angle between black lines) is collected, resulting in low reflectance. RPE is present but also degenerating. D. Because ORT cone IS contain many dispersed mitochondria, which reflect light (red arrows), OCT renders ORT with a hyperreflective border. Dotted circle represents ELM of ORT with the number of cones reduced for clarity. RPE is absent. Cells: RPE, retinal pigment epithelium; C, cone

photoreceptor (IS, inner segments; OS, outer segments); R, rod photoreceptor; H, horizontal cell; B, bipolar cell; M, Müller cell; Am, amacrine cell; DA, displaced amacrine cell; G, ganglion cell. Layers: ChC, choriocapillaris; BrM, Bruch's membrane; ELM, external limiting membrane; ONL, outer nuclear layer; OPL, outer plexiform layer; INL, inner nuclear layer; IPL, inner plexiform layer; GCL, ganglion cell layer; NFL, nerve fiber layer; ILM, inner limiting membrane. Drawings are not to scale. Reprinted with permission by Litts et al.[16]

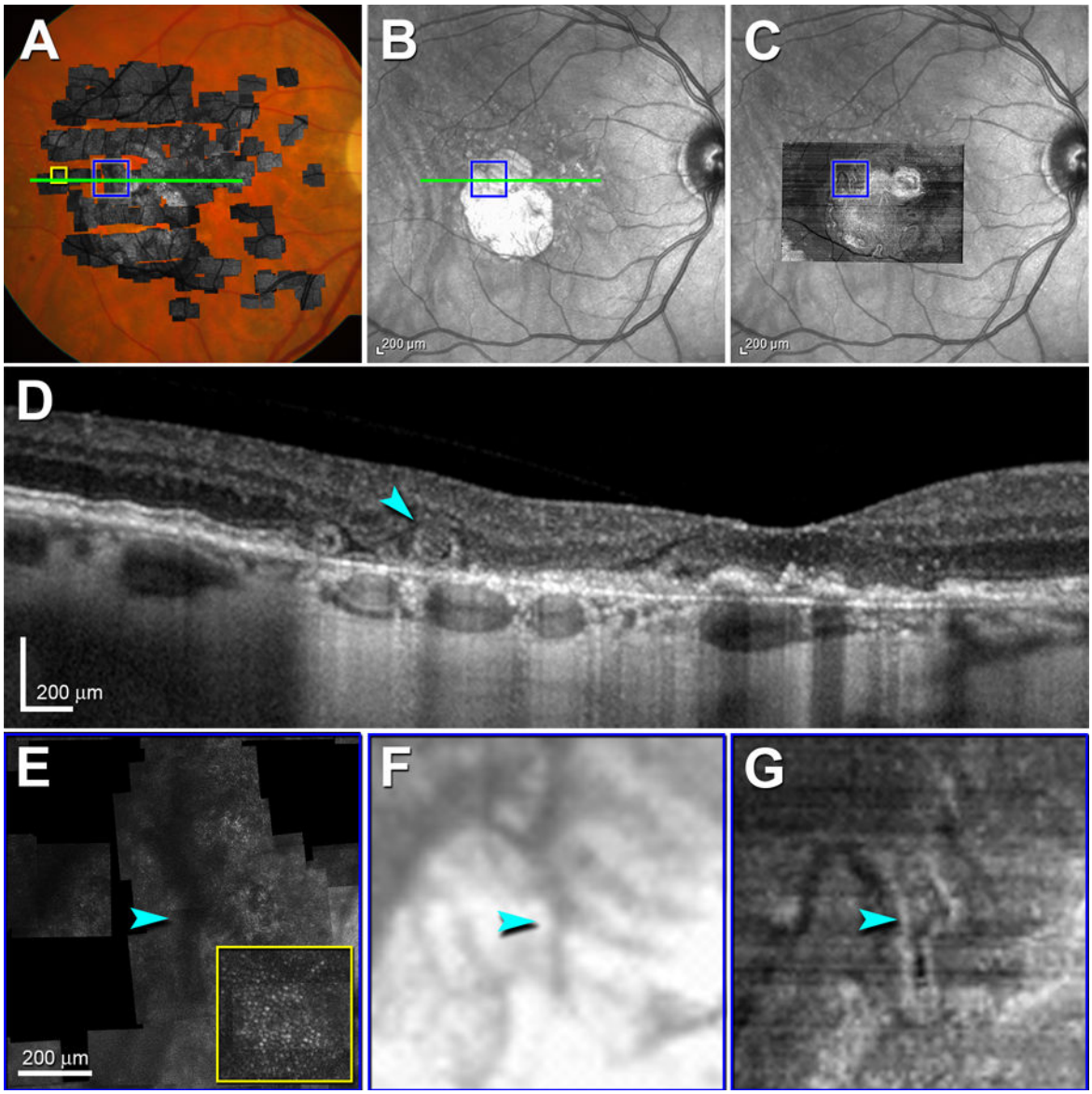

Figure 8. Outer retinal tubulation (ORT) in geographic atrophy secondary to age-related macular degeneration by multimodal imaging

This ORT is closed and perilesional.[138] A. Adaptive optics scanning laser ophthalmoscopy montage in grayscale overlaid on color fundus photograph of right eye from a 66- year-old woman (ORT-134) diagnosed with AMD. B. Near infrared reflectance (NIR) image. C. En face view from SD-OCT transverse reconstruction of high density B-scans through center of ORT overlaid on NIR image. Higher magnification of ORT in blue boxes and waveguiding cones in yellow box are in E– G. D. Spectral domain optical coherence tomography B-scan taken through green line in A–B shows location of ORT (cyan arrowhead). Higher magnification of ORT and waveguiding cones in yellow box by AOSLO (E), IR (F), and en face SD-OCT (G). Cyan arrowheads in E–G point to level of SD- OCT B-scan in D. Side of yellow box inset is 200 mm. Reprinted with permission from Litts et al.[16]

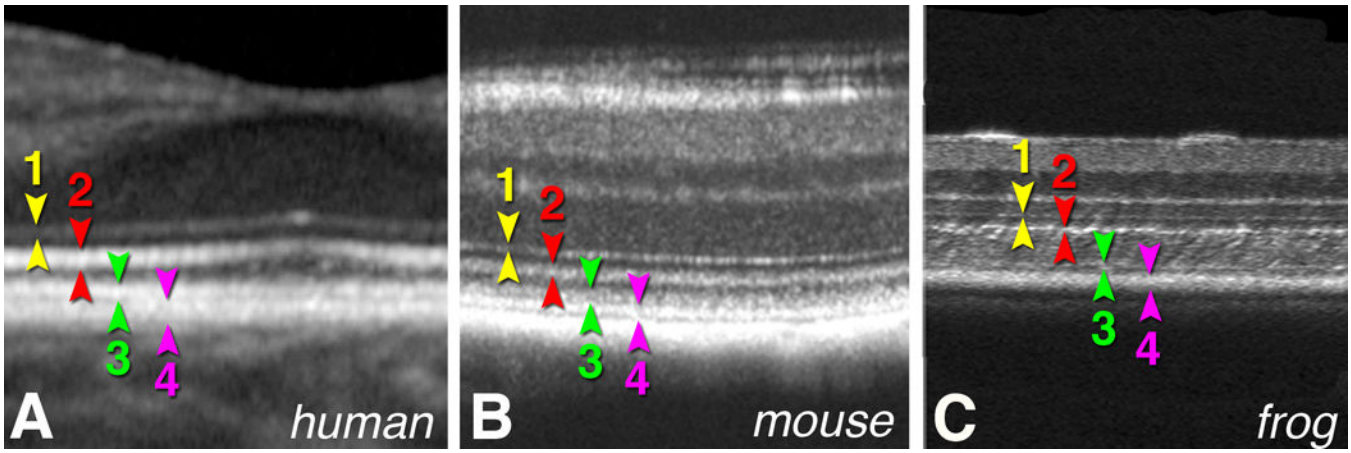

Figure 9. Hyperreflective outer retinal band in SDOCT in three species

A. Human fovea B. Mouse retina C. Frog retina. 1, external limiting membrane; 2, ellipsoid zone; 3, interdigitation zone; 4, retinal pigment epithelium/Bruch's complex. Mouse image courtesy of Steven Pittler, PhD; Department of Vision Science University of Alabama at Birmingham (NIH grant EY018143; P30 EY003039); frog image courtesy of Xincheng Yao, PhD; Department of Biomedical Engineering; University of Illinois at Chicago)

Table 1

Naming of Band 2 from 1995–2015

	1995–2006		2007–2009		2010–2011			2012		2013		2014		2015	Total
IS/OS junction or IS/OS interface	15	57.7%	13	68.4%	24	72.7%	11	55.0%	10	62.5%	1	12.5%	0	0.0%	74
Connecting cilium	2	7.7%	2	10.5%	2	6.1%	0	0.0%	0	0.0%	0	0.0%	0	0.0%	6
Indicated between IS and OS but not named	2	7.7%	1	5.3%	0	0.0%	0	0.0%	0	0.0%	0	0.0%	0	0.0%	3
RPE	2	7.7%	0	0.0%	0	0.0%	0	0.0%	0	0.0%	0	0.0%	0	0.0%	2
High reflectance band	1	3.8%	0	0.0%	1	3.0%	0	0.0%	0	0.0%	0	0.0%	0	0.0%	2
IS	1	3.8%	1	5.3%	0	0.0%	0	0.0%	1	6.3%	0	0.0%	0	0.0%	3
OS	1	3.8%	1	5.3%	1	3.0%	0	0.0%	0	0.0%	0	0.0%	0	0.0%	3
IPRL (interface of photoreceptor layer)	0	0.0%	0	0.0%	2	6.1%	0	0.0%	0	0.0%	0	0.0%	0	0.0%	2
ISe	0	0.0%	0	0.0%	0	0.0%	3	15.0%	3	18.8%	2	25.0%	3	7.1%	11
Ellipsoid Zone	0	0.0%	0	0.0%	0	0.0%	1	5.0%	1	6.3%	2	25.0%	4	9.5%	8
Other*	1	3.8%	1	5.3%	3	9.1%	2	10.0%	1	6.3%	1	12.5%	5	11.9%	14
Visible but not named	1	3.8%	0	0.0%	0	0.0%	3	15.0%	0	0.0%	2	25.0%	30	71.4%	36
Total Illustrations	26	100.0%	19	100.0%	33	100.0%	20	100.0%	16	100.0%	8	100.0%	42	100.0%	164

Publications including OCT scans of normal human or macaque retina with visible or labeled hyperreflective outer retinal bands from JAMA Ophthalmology (formerly Archives of Ophthalmology), British Journal of Ophthalmology, Ophthalmology, American Journal of Ophthalmology, Retina, Investigative Ophthalmology and Visual Science, and Optics Express.

*Other: outer retinal complex (2005), photoreceptor segment layer (2009), outer retinal boundary (2010), photoreceptor layer (2011), ELM (2011), Ellipsoid layer (2013), OS (2014), boundary of myoid and ellipsoid of inner segments (2015), Band 2 (2015), PR1 (2015), Ellipsoid (2015), Ellipsoid region (2015)